IVYSPRING INTERNATIONAL PUBLISHER

Theranostics

2019; 9(6): 1538-1549. doi: 10.7150/thno.30353

Research Paper

Anti-tumor effects and potential therapeutic response biomarkers in α-emitting *meta*-^{211}At-astato-benzylguanidine therapy for malignant pheochromocytoma explored by RNA-sequencing

Yasuhiro Ohshima[1*], Nobuaki Kono[2*], Yuichiro Yokota[1*], Shigeki Watanabe[1], Ichiro Sasaki[1], Noriko S. Ishioka[1], Tetsuya Sakashita[1]✉, Kazuharu Arakawa[2,3]✉

1. Department of Radiation-Applied Biology Research, Quantum Beam Science Research Directorate, National Institutes for Quantum and Radiological Science and Technology, 1233 Watanuki, Takasaki, Gunma 370-1292, Japan.
2. Institute for Advanced Biosciences, Keio University, 246-2 Mizukami, Kakuganji, Tsuruoka, Yamagata, 997-0052, Japan
3. Faculty of Environment and Information Studies, Keio University, 5322 Endo, Fujisawa, Kanagawa, 252-0882, Japan

*Co-first authors

✉ Corresponding authors: Kazuharu Arakawa, Ph.D., E-mail: gaou@sfc.keio.ac.jp; Phone: +81-235-29-0571. Tetsuya Sakashita, Ph.D., E-mail: sakashita.tetsuya@qst.go.jp; Phone: +81-27-346-9460.

Received: 2018.10.01; Accepted: 2019.01.04; Published: 2019.02.27

Abstract

Targeted α-particle therapy is a promising option for patients with malignant pheochromocytoma. Recent observations regarding *meta*-^{211}At-astato-benzylguanidine (^{211}At-MABG) in a pheochromocytoma mouse model showed a strong anti-tumor effect, though the molecular mechanism remains elusive. Here, we present the first comprehensive RNA-sequencing (RNA-seq) data for pheochromocytoma cells based on *in vitro* ^{211}At-MABG administration experiments. Key genes and pathways in the tumor α-particle radiation response are also examined to obtain potential response biomarkers.

Methods: We evaluated genome-wide transcriptional alterations in the rat pheochromocytoma cell line PC12 at 3, 6, and 12 h after ^{211}At-MABG treatment; a control experiment using ^{60}Co γ-ray irradiation was carried out to highlight ^{211}At-MABG-specific gene expression. For comparisons, 10% and 80% iso-survival doses (0.8 and 0.1 kBq/mL for ^{211}At-MABG and 10 and 1 Gy for ^{60}Co γ-rays) were used.

Results: Enrichment analysis of differentially expressed genes (DEGs) and analysis of the gene expression profiles of cell cycle checkpoints revealed similar modes of cell death via the p53-p21 signaling pathway after ^{211}At-MABG treatment and γ-ray irradiation. The top list of ranked DEGs demonstrated the expression of key genes on the decrease in the survival following ^{211}At-MABG exposure, and four potential genes (*Mien1*, *Otub1*, *Vdac1* and *Vegfa* genes) of ^{211}At-MABG therapy. Western blot analysis indicated increased expression of TSPO in ^{211}At-MABG-treated cells, suggesting its potential as a PET imaging probe.

Conclusion: Comprehensive RNA-seq revealed contrasting cellular responses to γ-ray and α-particle therapy, leading to the identification of four potential candidate genes that may serve as molecular imaging and ^{211}At-MABG therapy targets.

Key words: α-particle, *meta*-^{211}At-astato-benzylguanidine, RNA-sequencing, pheochromocytoma, PET imaging, radionuclide therapy

Introduction

Pheochromocytomas (PCCs) are rare neuroendocrine tumors with malignant progression that account for approximately 30% of extra-adrenal PCCs [1]. Some malignant PCCs exhibit systemic metastasis, and clinical improvement with β-emitting *meta*-^{131}I-iodo-benzylguanidine (^{131}I-MIBG) constitutes a stage

of partial remission in metastatic PCC [2]. Recently, we reported strong anti-tumor effects of α-emitting *meta*-^{211}At-astato-benzylguanidine (^{211}At-MABG) in a PCC mouse model, suggesting a potential option for targeted α therapy (TAT) for patients with malignant PCC [3]. Nonetheless, very little is known about the molecular mechanism of the therapeutic effects of ^{211}At-MABG compared with photon-radiation therapy [4]. To avoid unintended consequences, a better understanding of the molecular basis of such therapeutic effects is necessary for the clinical implementation of ^{211}At-MABG therapy in malignant PCC.

Theranostics, which combines specific targeted therapy and specific targeted diagnosis, is important for TAT, especially with regard to diagnosis. *In vivo* localization is one of main components of theranostic diagnosis, which includes Cherenkov luminescence imaging of ^{225}Ac-labeled compounds [5] and a Compton camera for ^{211}At-labeled compounds [6]. Another main component is the real-time dynamic imaging proposed by Paulmurugan et al. [7]. Overall, understanding or assessing therapeutic tumor responses, e.g., through inflammation biomarkers, is crucial [8]; although both components are required for TAT, few studies have focused on the latter. Accordingly, in this study, we explored therapeutic response biomarkers.

Post-genome sequencing technologies have rapidly developed in the last ten years, and next-generation sequencing (NGS) is a powerful tool for unraveling the molecular basis of rare genetic diseases [9]. Furthermore, RNA-sequencing (RNA-seq) using NGS provides a more precise transcription profile compared to other methods [10], and this approach may contribute to the search of TAT-response biomarkers.

Prior to the advent of RNA-seq, some *in vitro* TAT studies utilized microarray technology to measure gene expression and identify differentially expressed genes (DEGs) participating in DNA repair, cell cycle checkpoints, and apoptosis [11, 12, 13], as shown by photon radiation therapy [4]. For example, Seidl *et al.* reported novel gene regulation of TAT with high significance, identifying *COL4A2*, *NEDD9*, and *C3* genes as being continuously upregulated; however, their specific functions in the response to high linear-energy-transfer ionizing radiation (IR) remain unknown [11]. Comprehensive RNA-seq analysis can now provide a wide dynamic range and great statistical precision with an increasing number of time points and biological replicates, thus allowing precise identification of key genes of TAT [14].

In this study, we examined gene expression profiles via RNA-seq in rat PCC cells to elucidate the molecular mechanism of ^{211}At-MABG therapeutic effects compared with those of photon (γ-ray) irradiation under the expected conditions in line with TAT and the conventional radiotherapy. We further explored key genes in the tumor response to radiation as well as potential molecular therapeutic biomarkers for malignant PCC.

Materials and Methods

Cell culture

PC12, a rat pheochromocytoma cell line, is a representative cell line for malignant PCC [15] with long history of being the model for nuclear medicine studies, including the contribution to the preclinical study of MIBG therapy [16]. PC12 was purchased from Japanese Collection of Research Bioresources (IFO50278, Osaka, Japan), and cultured as previously reported [3] (Supplementary materials and methods).

^{211}At-MABG treatment, γ-ray irradiation and dose estimation

^{211}At-MABG was synthesized as previously described [3]. The radioactivity of ^{211}At ($T_{1/2}$ = 7.2 h) was measured from γ-rays emitted in ^{211}At decay using a high-purity germanium detector. We estimated the absorbed dose of ^{211}At-MABG-treated cells using a published method [17], with some modifications (Supplementary materials and methods), as based on cellular uptake and release experiments, a parameter of energy per decay for ^{211}At [18] and a real-coded genetic algorithm to estimate parameters [19]. Stable-iodine labeled MIBG was used for the nonradioactive experiments of ^{211}At-MABG (MIBG-control; Supplementary materials and methods). The ^{60}Co source at the Takasaki food irradiation facility was used for γ-ray irradiation, and the dose-rate distribution was routinely monitored using polymer-alanine dosimeters (Hitachi Cable, Ltd., Tokyo, Japan). The absorbed dose of γ-ray irradiated cells, assumed to be a water equivalent, was interpolated from routine monitoring data. PC12 cells were exposed to ^{211}At-MABG at concentrations of 0, 0.2, 0.6, 2.0 and 6.0 kBq/mL for 1 day or were irradiated with ^{60}Co γ-rays at doses of 0, 0.1, 0.3, 1, 3 and 10 Gy for 12 min time periods. **Figure 1** shows the experimental design for ^{211}At-MABG treatment and ^{60}Co γ-rays irradiation. Cell survival assays were carried out as previously reported (Supplementary materials and methods).

RNA extraction and sequencing

A sample of 10^6 harvested cells was resuspended in TRIzol (Thermo Fisher Scientific, Waltham, MA, USA), and RNA was extracted using the Direct-zol RNA kit (Zymo Research Corp, Orange, CA, USA)

according to the manufacturer's protocol. A sequencing library was prepared using the NEBNext, Ultra RNA Library Prep Kit (New England Biolabs, Ipswich, MA). Multiplex sequencing was performed with the High Output Mode regents of the NextSeq 500 instrument (Illumina Inc., San Diego, CA) using 75 cycles for control and γ-ray-irradiated samples and 300 cycles for ^{211}At-MABG treated samples. These sequencing data sets were deposited (and are available) at the DNA Data Bank of Japan (DDBJ: http://www.ddbj.nig.ac.jp/) Sequence Read Archive under Accession number DRA007102 and DRA007735.

Differential expression analysis

Sequencing reads were aligned to the rat Ensembl Rnor 6.0 reference genome obtained from Ensembl using TopHat2 v2.0.14 with a default setting [20]. The aligned reads were assembled using Cufflinks v2.2.1 [21] with an annotation file (Rnor 6.0.83), along with estimation of the abundance of each transcript. Expression levels were calculated as fragments per kilobase of exon per million fragments mapped (FPKM). Assemblies of three replicates were combined using Cuffmerge v1.0.0. Differential expression analysis of each combination was performed using Cuffdiff v2.2.1 [22].

For pathway enrichment analysis, reference genes were first matched to KEGG (Kyoto Encyclopedia of Genes and Genomes) orthology using the KEGG KAAS web service [23], and enrichment of pathways for each time point was assessed using a custom Perl script in the G-language Genome Analysis Environment [24], utilizing Fisher's exact test of the R package (https://www.r-project.org) with Bonferroni correction of *p*-values for multiple testing. For both differential gene expression and pathway enrichment analysis, a false discovery rate (FDR) threshold of 0.05 was used. Disease-related pathways with a pathway map ID greater than 5000 were omitted.

Configuration of the gene regulatory network and representative DEGs

A gene regulatory network was obtained from the KEGG pathway map [23]. Genes involved in the regulatory network were screened according to the following conditions: 1. at least twofold highly expressed genes in the treatment; 2. at least FPKM > 1 for all conditions; 3. overrepresentation in at least one of twelve conditions (γ-ray irradiation, ^{211}At-MABG treatment, two survival rates, and three time points) compared with the corresponding controls; 4. presence of the canonical gene name.

Using similar conditions, except for the 3rd, representative genes with significant changes in expression were screened between the γ-ray and ^{211}At-MABG treatments. The 3rd condition was modified with a comparison of combination treatments: e.g., for representative DEGs of ^{211}At-MABG treated cells between 80% and 10% survival doses at each time point, we used the condition of DEGs overrepresented in at least one of the two conditions (including the two survival rates).

Flow cytometry and western blot analysis

Cell cycle distributions among cells treated with ^{211}At-MABG (0.6 kBq/mL) for 24 h and 24 h post-irradiated with γ-ray (10 Gy) were analyzed using flow cytometry. Cells were collected and fixed in 70% ethanol overnight, treated with RNase for 20 min before the addition of 5 μg/mL of propidium iodide and analyzed by flow cytometry (EC-800, Sony, Tokyo, Japan). Western blot analysis of cells treated with ^{211}At-MABG (0.8 kBq/mL) for 6, 12 and 24 h was performed as previously described (Supplementary materials and methods) [25].

Statistical analysis

The computer program (ORIGIN, MicroCal Software, Inc., MA, USA) was used for non-linear curve fitting.

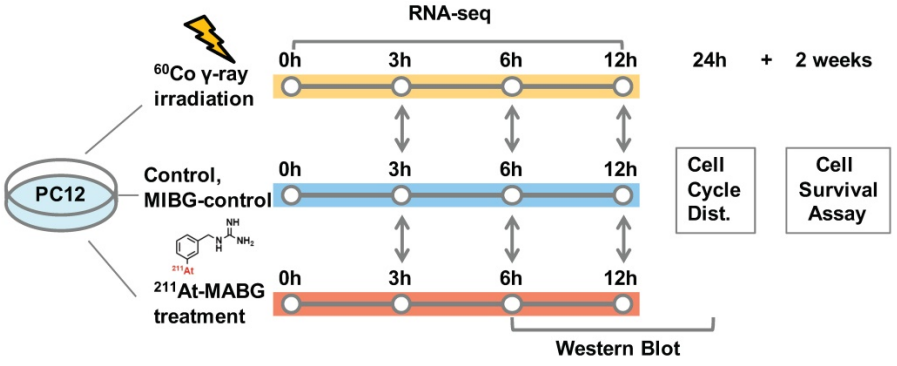

Figure 1. Experimental design for ^{211}At-MABG treatment and ^{60}Co γ-rays irradiation. Comparative RNA-seq analysis between control, γ-ray-irradiated and ^{211}At-MABG-treated samples was performed at 3, 6 and 12 h. MIBG-control additional experiment was also carried out in the same time course. Cell cycle distribution was measured at 24 h, and a cell survival assay was performed after 2 weeks of incubation.

Results

Iso-survival dose and experimental design for ^{211}At-MABG treatment and ^{60}Co γ-ray irradiation

To compare the biological effects of two types of radiation, we first evaluated the 10% and 80% iso-survival doses of ^{60}Co γ-ray irradiation and ^{211}At-MABG treatment for PC12 cells. For this study, we used the acute irradiation for ^{60}Co γ-rays to imitate conventional radiation therapy.

Cells irradiated with γ-rays exhibited a log-linear relationship between the surviving fraction (*SF*) and the absorbed dose (**Figure 2**), with 10% and 80% iso-survival doses of γ 10 Gy (*SF* = 10.8%) and 1 Gy (*SF* = 80.1%), respectively. The absorbed dose of ^{211}At-MABG by treated cells was estimated using a published method [19], with some modifications (Supplementary materials and methods). When cells were exposed to ^{211}At-MABG at the initial concentration of 1.0 kBq/mL, the absorbed dose was estimated to be 4.31 Gy. Using this estimation, the relationship between the *SF*s of 0, 0.2, 0.6, 2.0 and 6.0 kBq/mL and the absorbed dose displayed a sigmoidal curve (**Figure 2**). The 10% and 80% iso-survival doses of ^{211}At-MABG were set to 0.8 kBq/mL (3.5 Gy; *SF* = 9.8%) and 0.1 kBq/mL (0.4 Gy; *SF* = 82%), respectiveely, and we designed the time-course of RNA-seq analysis accordingly (**Figure 1**). In general, IR- induced DNA damage causes an increase or decrease in gene expression several hours post-irradiation. Indeed, ^{60}Co γ-rays and α-particles emitted from ^{211}At induced significant alterations in gene expression several hours after treatment [14]. Thus, we used three time points for RNA-seq analysis at 3, 6 and 12 h after ^{60}Co γ-ray irradiation and the start of ^{211}At-MABG exposure.

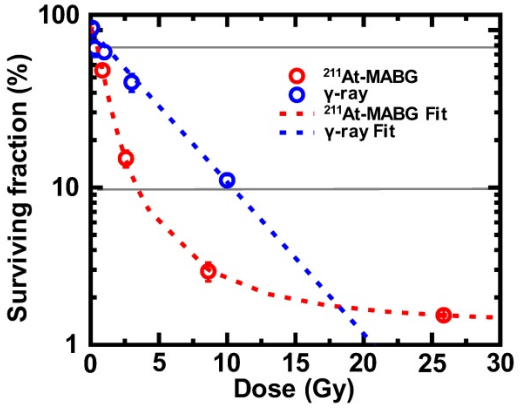

Figure 2. Iso-survival dose for ^{211}At-MABG treatment and ^{60}Co γ-rays irradiation. Surviving fraction (*SF*) after ^{211}At-MABG treatment and ^{60}Co γ-rays irradiation in PC12 cells. The *SF* of ^{211}At-MABG treatment demonstrated a sigmoidal curve (^{211}At-MABG Fit)—that is, *SF* (%) = 1.3 + (100.0 – 1.3) / (1.0 + (*Dose* (Gy) / 0.97)$^{1.9}$) (the correlation coefficient square, R^2 = 1.00). The *SF* of ^{60}Co γ-ray irradiation showed a log-linear relationship (γFit)—that is, *SF* (%) = 100.0 exp (-0.22 * *Dose* (Gy)) (R^2 = 0.98). Thin lines indicate 10% and 80% survival.

Comprehensive RNA-seq analysis of ^{211}At-MABG-treated and ^{60}Co γ-ray-irradiated PC12 cells

We employed a transcriptomic approach to observe changes in gene expression in PC12 cells at iso-survival doses of 10% and 80%, and a minimum of 7 million reads were sequenced for each condition in three replicates (**Figure 3**). Overall transcriptome profiles were consistent among the replicates and strikingly distinct among the three treatment conditions (control, γ-ray irradiation, ^{211}At-MABG treatment), essentially regardless of the survival rate or time point. Although γ-ray-irradiated samples shared a proportion of gene clusters showing similar expression levels as the control, ^{211}At-MABG treatment resulted in vastly different profiles, with the early (3 h) response to weak irradiation (80% survival) exhibiting a very weak correlation (approximately 0.2 in Pearson correlation) with the 3-h control conditions (**Figure S3**). These differential expression patterns were further supported by the number of DEGs, as summarized in **Figure S4**. The numbers of DEGs were highly consistent among the different time points, with the number of DEGs at 80% survival after ^{211}At-MABG treatment (5,881, 5,198 and 5,304 genes at 3, 6 and 12 h, respectively) all surpassing those of 10% survival after γ-ray irradiation (4,438, 3,812 and 4,414 genes at 3, 6 and 12 h, respectively). MIBG-control experiments did not show the same transcriptome profiles treated with ^{211}At-MABG and ^{60}Co γ-rays (**Figure S5**), and showed very limited number of DEGs, where the maximum number of DEGs exceeding fold change > 2 being 70 (**Figure S6**). Significant changes in gene expression at 80% survival after γ-ray irradiation (1,974, 1,731 and 2,590 genes at 3, 6 and 12 h, respectively) were largely fewer than half under all other conditions. Therefore, the intracellular response to these two conditions appears to be contrasting, presumably providing an explanation for the different tumor responses to X/γ-ray and TAT therapies. We thus focus on the difference in responses, in other words, the more than 5,000 DEGs between the two irradiation conditions.

Enrichment in biological processes in DEGs was next examined using KEGG pathway enrichment analysis (**Figure 4**). γ-Ray irradiation predominantly resulted in under-representation of DNA damage repair (base excision repair, nucleotide excision repair, mismatch repair, and homologous recombination) and cell cycle-related (DNA replication, cell cycle) pathways, suggesting cell cycle arrest and stalling of DNA replication. In contrast, ^{211}At-MABG treatment did not result in these under-representations, except for 6 or 12 h of 10% survival; however, over-representation of protein turnover

(ribosome biogenesis, RNA transport, ubiquitin mediated proteolysis, and protein processing in endoplasmic reticulum) was observed. Only the p53 signaling pathway was over-represented in cells treated with both γ-ray irradiation and ^{211}At-MABG.

Cell cycle checkpoints and the p53-p21 pathway

The pathway enrichment analysis indicated cell cycle arrest, stalling of DNA replication and activation of p53 signaling. To understand how γ-ray irradiation and ^{211}At-MABG treatment regulate the cell cycle, we screened well-known genes that participate in DNA damage-dependent G1/S and G2/M checkpoints using the present configuration (see a description in the Materials and methods). The relationships among *Tp53*, *Mdm2*, *Chek2*, *Cdkn1a*, *Skp2*, *Cdk2*, *Ccne1,2*, *Rb1*, *Gadd45a,g*, *Cdc25b*, *Plk1*, *Cdk1* and *Ccnb1* transcripts are illustrated in **Figure 5A**. Despite differences in the gene expression pattern for the early response and delayed induction between both treatments (**Figure S7**), an overview of the selected gene expression levels resulted in a similar expression profile (**Figure 5A**). The expression levels of *Mdm2*, *Cdkn1a*, *Gadd45a,g* and *Rb1* genes increased, whereas those of the other genes decreased (**Figure 5A**), suggesting activation of G1/S and G2/M checkpoints via the p53 pathway. Flow cytometry analysis supported the transcriptomic results, demonstrating a decrease and increase in the ratio of S- and G2/M-phase cells, respectively (**Figure 5B**). These results show that the p53 pathway is an important cell cycle regulator in γ-ray irradiation and ^{211}At-MABG treatment. Nonetheless, transcriptional activation of the *Cdkn1a* gene is also regulated via p53-independent pathways [26] (**Figure 5C**). In addition, we found reduced expression of suppressor APC-MYC pathway components and increased *Klf6* expression to be associated with transcriptional regulation of CDKN1A (**Figure 5C-D**). Taken together, our data suggest that the p53 signaling pathway via DNA damage and associated signals regulate the PC12 cell cycle after γ-ray irradiation and ^{211}At-MABG treatment.

Representative DEGs of ^{211}At-MABG-treated cells between 80% and 10% survival doses

Analysis of cell cycle checkpoints demonstrated a similar response to γ-ray irradiation and ^{211}At-MABG treatment, yet the DEGs associated with ^{211}At-MABG therapeutic effects were unclear. Therefore, we investigated representative DEGs that contribute to a decrease in survival after ^{211}At-MABG treatment.

The number of representative DEGs between 80% and 10% survival increased in a time-dependent manner (11 genes at 3 h post-treatment to 60 genes at 12 h). **Table 1** classifies the representative DEGs into 5 categories at each time point. The top-ranking genes were *Nudt6* (7.9-fold increase), *Eda2r* (5.3-fold increase) and *Inmt* (5.3-fold increase) at 3, 6 and 12 h post-^{211}At-MABG treatment, respectively. *Nudt6* is suggested to play a role in cell proliferation [27], and *Eda2r* is reported to induce apoptosis and prevent cell adhesion through the p53-regulated anoikis pathway [28]. *Inmt* codes for an indolethylamine-*N*-methyltransferase (INMT), which produces *N*,*N*-dimethyltryptamine (DMT) [29]; although the role of endogenous DMT has not yet been established, exogenous DMT acts as an inhibitor of peripheral monoamine oxidase [30]. Representative DEGs found at all time points included *Gdf15*, *Fam212b*, *Cdkn1a*, *Enc1* and *Tp53inp1* (Table 2), all of which are target genes of activated p53 [31]. These DEGs provide a straightforward description of the state of PC12 cells incorporating ^{211}At-MABG, i.e., cell cycle regulation and cell death induction.

Table 1. ^{211}At-MABG induces a time-dependent shift in representative DEGs between 80% and 10% survival experiments.

	3 h post-treatment (11 genes)*1			6 h post-treatment (52 genes)*1			12 h post-treatment (60 genes)*1		
	Gene name	LogFC*2	Function	*Gene name*	LogFC*2	Function	*Gene name*	LogFC*2	Function
Cell cycle	*Nudt6*	+2.976 (1)	Cell proliferation	*Ptprv*	+1.889 (6)	G1/S checkpoint	*Ptprv*	+2.022 (5)	G1/S checkpoint
				Ccng1	+1.412 (12)	G2/M checkpoint	*Ccng1*	+1.412 (25)	G2/M checkpoint
				Plk2	+1.055 (44)	Spindle checkpoint	*Plk2*	+1.182 (43)	Spindle checkpoint
Cell death				*Eda2r*	+2.403 (1)	Apoptosis and prevention of cell adhesion	*Eda2r*	+2.006 (6)	Apoptosis and prevention of cell adhesion
				Aen	+1.354 (16)	Apoptosis	*Atg9b*	+1.991 (7)	Autophagy
				Btg2	+1.351 (18)	Apoptosis	*Gsdmd*	+1.669 (13)	Programmed cell death
DNA repair	*Aplf*	+1.381 (5)	DNA repair	*Ier5*	+1.201 (28)	DNA repair	*Mgmt*	+1.290 (31)	DNA repair
	Fam175a	+1.018 (11)	DNA repair with BRCA1	*Rnf169*	+1.028 (48)	Homologous recombination	*Xrcc1*	+1.044 (54)	Base excision repair
Metastasis				*Adam8*	+1.882 (7)	Invasion	*Adam8*	+2.164 (3)	Invasion
				Jam3	+1.177 (30)	Adhesion	*Mmp2*	+1.851 (8)	Metastasis
Others				*Inmt*	+1.631 (9)	Methyltransferase	*Inmt*	+2.403 (1)	Methyltransferase
				Trim7	+1.315 (21)	Proliferation, Apoptosis	*Lrrc25*	+1.682 (11)	Inflammation, Autophagy

*1 Number of DEGs. *2 The number in parentheses indicates the rank

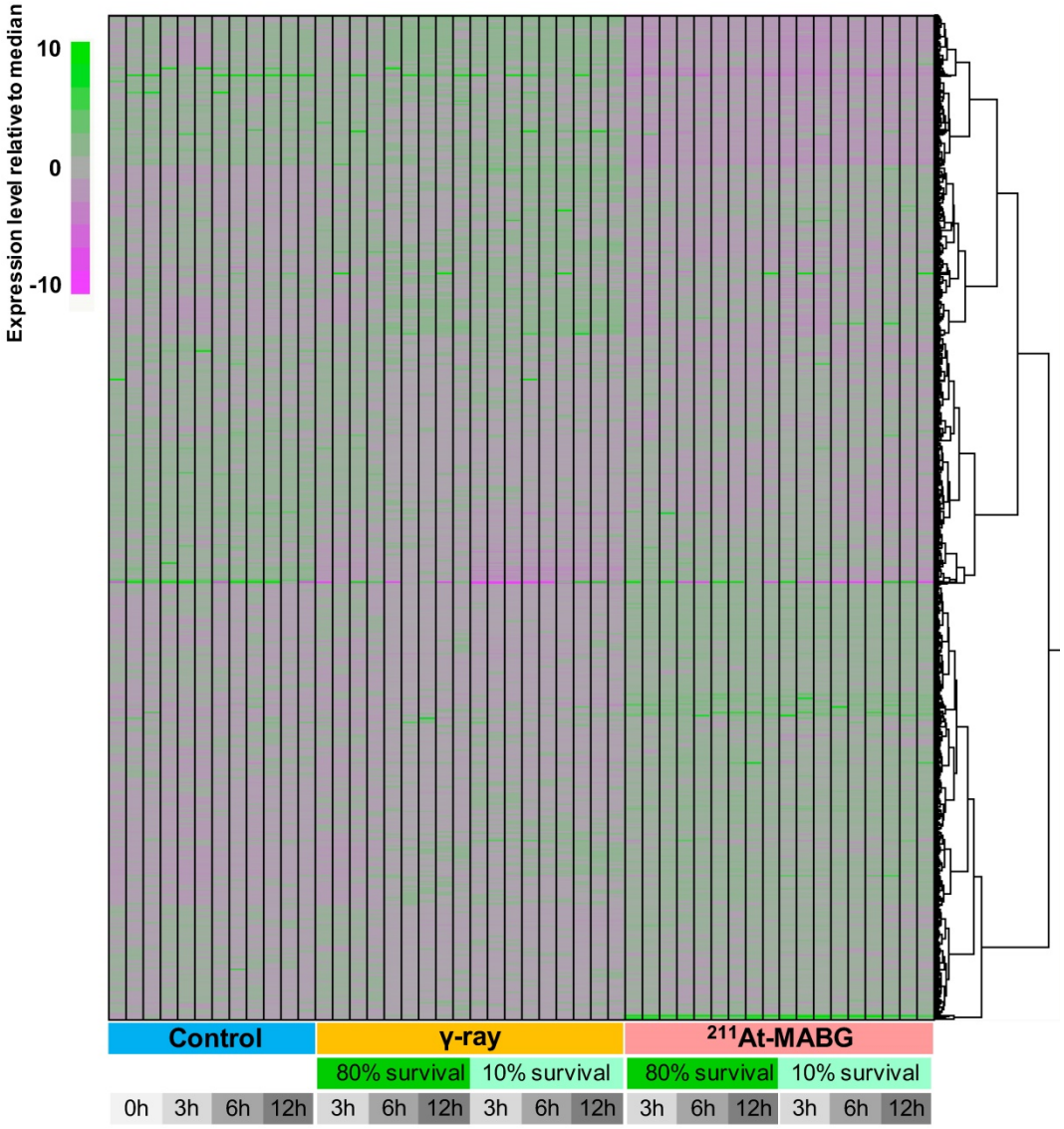

Figure 3. Heatmap clustering of all RNA-seq data used in this analysis. The expression level of all genes with TPM (Transcript Per Million) > 5 in any condition is normalized relative to the median expression level for each gene. The expression level was calculated using kallisto software (v.0.42.4). Regardless of the time point or survival rate, the three conditions (control, γ-ray irradiation, ^{211}At-MABG treatment) showed distinct expression patterns, with ^{211}At-MABG treatment showing greater variability.

Furthermore, representative DEGs in PC12 cells at each time point exhibited varying gene expression profiles. At 3 h post-treatment, *Aplf* and *Fam175a* genes were observed, with *Fam175a* suggesting the involvement of homologous recombination (HR). DNA-repair related genes were continuously expressed after 3 h post-treatment (*Ier5*, *Rnf169*, *Mgmt* and *Xrcc1*of **Table 1**); various genes were represented at 6 and 12 h post-treatment. In the cell cycle category, *Ptprv* for the G1/S checkpoint, *Ccng1* for the G2/M checkpoint and *Plk2* for the spindle checkpoint were highly represented, in agreement with the results shown in **Figure 5A-B**. Regarding the category of cell death, apoptosis-related genes (*Aen*, *Btg2* and *Trim7*) were expressed from 6 h post-treatment, whereas autophagy- and other-related genes (*Atg9b*, *Gsdmd* and *Lrrc25*) ranked in the top 30 at 12 h post-treatment. Moreover, ^{211}At-MABG treatment induced metastasis-related gene expression (*Adam8*, *Jam3* and *Mmp2*). Therefore, representative DEGs of ^{211}At-MABG-treated cells between 80% and 10% survival doses effectively highlight the expression of key genes associated with ^{211}At-MABG therapeutic and anti-therapeutic effects.

Potential therapeutic response biomarkers of ^{211}At-MABG

To investigate the different molecular mechanisms of ^{211}At-MABG treatment compared with photon (γ-ray) irradiation, we further screened for representative genes displaying changes in expression between γ-ray and ^{211}At-MABG treatments.

Representative DEG analysis revealed in 161 genes (**Table S1**), among which 26 showed a log fold change greater than 2 and 87 were highly abundant, with a maximum FPKM > 100. Thus, only 20 genes satisfied both conditions, with 10 annotated in KEGG pathways. We selected four of these genes, *Mien1*, *Otub1*, *Vdac1* and *Vegfa*, based on their possible contribution to the ^{211}At-MABG treatment response. Overall, their maximum log fold-changes in gene expression (15.5, 8.4, 9.5 and 6.9 vs. γ-ray irradiation; **Figure 6A**) and continuous high level of expression demonstrate the ^{211}At-MABG-specific response.

Mien1 encodes migration and invasion enhancer 1 (MIEN1), a factor regulating cytoskeletal-focal adhesion dynamics [32]. Ovarian tumor domain-containing ubiquitin aldehyde-binding protein 1 (OTUB1), which is encoded by *Otub1*, has a bilateral character, both inhibiting and promoting tumor growth [33, 34]. *Mien1* and *Otub1* genes may be important targets for better estimating prognosis of ^{211}At-MABG therapy. *Vdac1* and *Vegfa* are linked to feasibility analysis for imaging: a mitochondrial 18-kDa translocator protein (TSPO), which forms a complex with 32-kDa voltage-dependent anion channel 1 (VDAC1) [35], is a well-studied drug target for PET imaging [25] and we measured the large increases in gene and protein expressions (**Figure 6B-6C**). Vascular endothelial growth factor A (VEGFA) is also a reported target for PET imaging [34]. The features of these 4 potential ^{211}At-MABG-specific molecular biomarkers may help doctors in diagnosis and in predicting prognosis with ^{211}At-MABG therapy.

Discussion

In this work, we applied RNA-seq and showed contrasting gene expression patterns between ^{211}At-MABG treatment and γ-ray irradiation. Moreover, analysis of representative DEGs uncovered key gene expression associated with ^{211}At-MABG therapeutic effects and novel biomarkers for response to ^{211}At-MABG therapy (**Figure 7A**).

Potential biomarkers for imaging in ^{211}At-MABG therapy

CT or MRI and ^{123}I-MIBG are typically used to identify metastatic PCC [1, 2], and PET with ^{18}F-fluorodopamine, ^{18}F-fluorodopa, ^{18}F-fluorodeoxy-glucose and ^{11}C-hydroxyephedrine can be used as alternatives to ^{123}I-MIBG or ^{131}I-MIBG [1, 2]. These imaging procedures can be applied to diagnosis—e.g., localization of metastatic PCC—in ^{211}At-MABG therapy. However, there is no target to date for measuring the α-particle-induced tumor response, that is, a TAT-response biomarker. In this study, we found three potential genes, *Vdac1*, *Vegfa* and *Mmp2*, that may shed light on this issue.

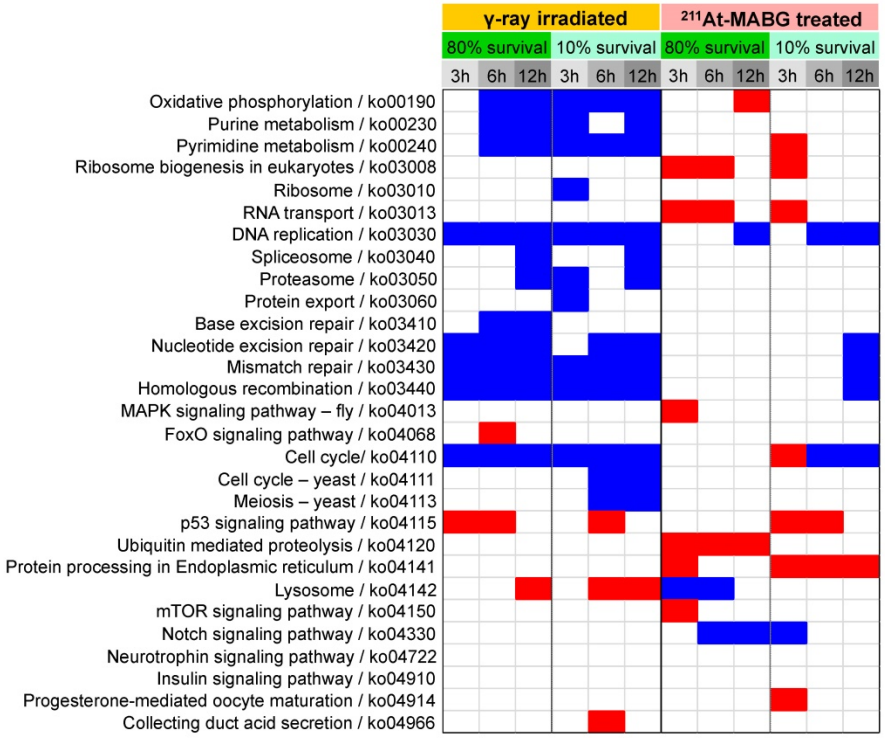

Figure 4. Enrichment of KEGG pathways in DEGs at each condition. KEGG (Kyoto Encyclopedia of Genes and Genomes) enrichment for differentially expressed genes (DEGs) was computed using Fisher's exact test with Bonferroni correction of *p*-values, where the corrected *p*-value < 0.05 is shown. KEGG pathways for human diseases are omitted. Red and blue squares represent positive and negative enrichment, respectively. γ-Ray-irradiated and ^{211}At-MABG-treated samples show contrasting enrichment of KEGG pathways.

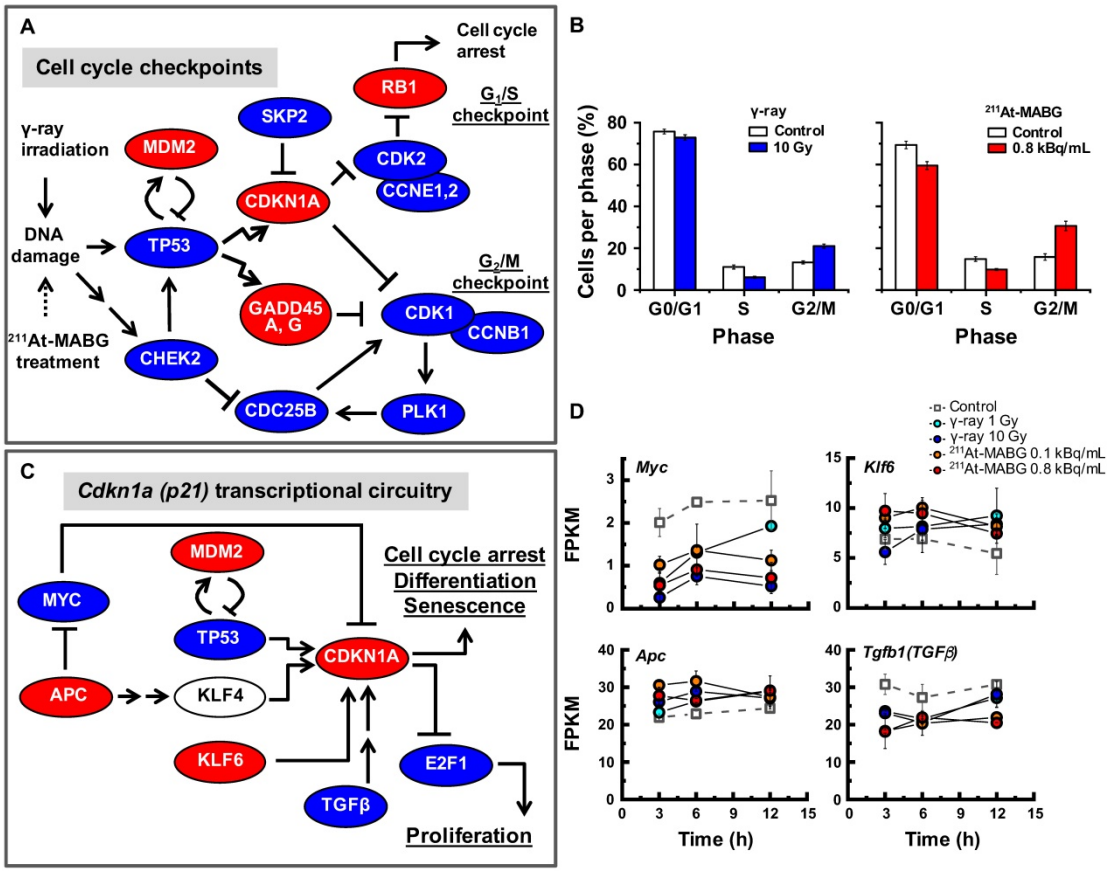

Figure 5. Cell cycle checkpoints, cell cycle distribution and the p53-p21 pathway. (A) The gene regulatory network for cell cycle checkpoints was configured with reference to the KEGG pathway map [17]. Red and blue ellipses represent the increase or decrease in gene expression (vs. control) after both ^{60}Co γ-ray irradiation and ^{211}At-MABG treatment, respectively. Both treatments showed similar gene expression profiles. **(B)** Cells per phase in % of 10% iso-survival experiments (left and right panels for γ-ray irradiation and ^{211}At-MABG treatment, respectively). The error bars indicate the standard error of mean. **(C)** *Cdkn1a* transcriptional circuitry [19]. Red and blue ellipses represent the increase or decrease in gene expression (vs. control), respectively. **(D)** Gene expression over time of *Myc*, *Apc*, *Klf6* and *Tgfb1* genes. The error bars represent standard deviation.

Vegfa specifically responds to MABG (**Figure 6A**) and is well known as a key imaging biomarker for tumor angiogenesis, *i.e.* tumor biomarker [36, 37]. We found that it was also potential response biomarker for ^{211}At-MABG therapy. HIF-1 [38] and MYC [39] activate *Vegfa* gene transcription. *Myc* gene may be not associated with tumor angiogenesis of MABG-treated PC12 cells, because of under-regulation of *Myc* gene expression (**Figure 5D**). There are many inhibitors of VEGF signaling; for example, sorafenib inhibits RAS/RAF/MEk/ERK effects on VEGFA [37]. Thus, inhibitor use and monitoring of VEGFA may be important for assessing tumor angiogenesis after ^{211}At-MABG therapy.

Overexpression of matrix metalloproteinases, e.g., MMP2 or MMP9, aids in prognosis for breast cancer patients [40], and in our study, the *Mmp2* gene was found to be representative at 12 h post-treatment (**Table 1**). Accordingly, evaluation of MMP2 response may be also important for prognosis after ^{211}At-MABG therapy.

Here, we propose *Tspo* as a potential imaging biomarker because it is related to VDAC1 [33]; TSPO is a well-known drug target for PET [25]. TSPO, VDAC1 and inner membrane adenine nucleotide transporter (ANT) form a complex at the mitochondrial membrane (**Figure 6B**) that functions as a REDOX regulator of cell mitophagy, inducing various oxidative stress responses, including apoptosis [35]. Levels of *Tspo*, *Vdac1* and *Ant* gene expression were significantly increased (**Figure 6A-6B**), and that of *Tspo* was initiated in the early phase after ^{211}At-MABG treatment and maintained over three time points in a dose-dependent manner (**Figure 6A-6B**). We also carried out western blot analysis, and levels of TSPO, detected at 18-19 kDa, increased over time in the 10% survival experiment (**Figure 6C**). ^{18}F-*N*-fluoroacetyl-*N*-(2,5-dimethoxybenzyl)-2-phenoxyaniline was reported to be a candidate probe for quantitative assessment of TSPO expression [25]. As PET signals from metastatic PCC can likely be detected *in vivo*, our results suggest that the PET imaging approach of assessing TSPO expression may detect the ^{211}At-MABG-induced tumor response and can provide indirect evidence of ^{211}At-MABG localization.

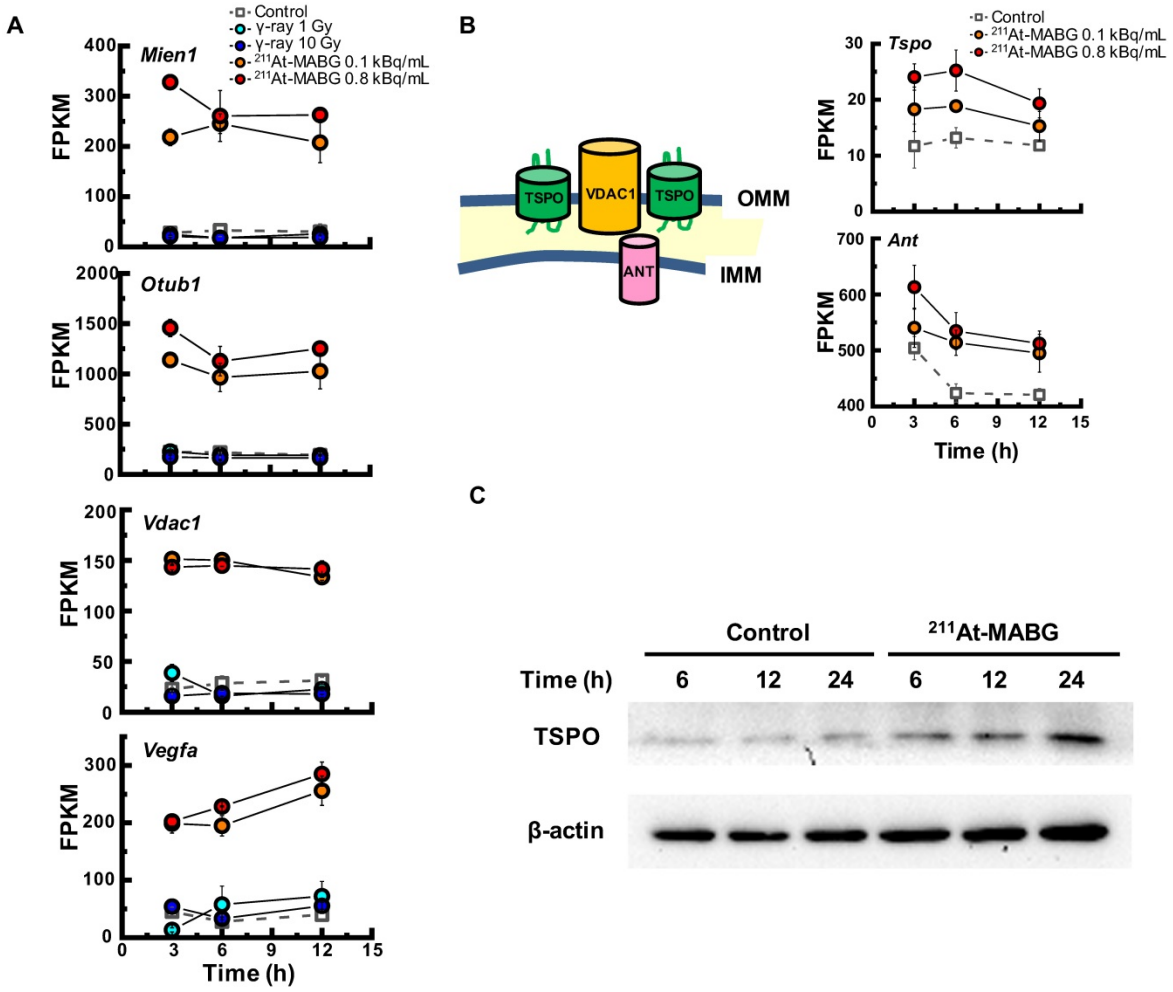

Figure 6. Potential molecular biomarkers for ^{211}At-MABG-therapy. (A) Gene expression according to the FPKM of *Mien1*, *Otub1*, *Vdac1* and *Vegfa* genes. Upregulated genes have a log fold change over two and a maximum FPKM above 100. **(B)** VDAC1-related molecules and gene expression. TSPO, VDAC1 and ANT in the mitochondrial membrane form a complex (left panel) and control the intracellular level of reactive oxygen species. Expression levels of upregulated *Tspo* and *Ant* genes (right panel). **(C)** Western blot analysis for TSPO was performed using PC12 cells collected at 6, 12 and 24 h post-^{211}At-MABG treatment. TSPO was detected at 18-19 kDa, and its expression was increased in a time-dependent manner. In **A** and **B**, error bars represent the standard deviation among the three replicates, and the symbols indicate the median value.

Biomarkers for better prognosis after ^{211}At-MABG therapy

Metastasis-related gene expression is important for prognosis. The present study showed metastasis-related genes, not only *Adam8*, *Jam3*, *Mmp2* and *Gdf15* listed in **Table 1** but also *Mien1* and *Otub1,* with high-level induction. ADAM8 promotes invasiveness and reduces patient survival in pancreatic cancer [41]. The peptide blocker BK-1361 may reduce the cellular activity of Adam8 [42]. In addition, inhibitors of MMP2 and GDF15 have been reported [43, 44], and a therapeutic target of MIEN1, microRNA miR-136, has been proposed [45]. Inhibitory drug and therapeutic targets of JAM3 and OTUB1 are not still understood, and in particular, the therapeutic effects of OTUB1 remain controversial.

OTUB1 is a deubiquitinating enzyme that stabilizes p53 by inhibiting the ubiquitin-conjugating enzyme (E2)-dependent ubiquitination involved in cell death and growth inhibition [33]. Despite a recent report that OTUB1 stabilizes MDMX and induces apoptosis [46], OTUB1 stabilizes proteins linked to cancer progression such as RAS and FOXM1 via deubiquitination and promotes tumor growth and invasion [34,47]. Indeed, high expression of OTUB1 is clinically associated with tumor invasion, metastasis, poor prognosis, and low patient survival [34]. These previous reports indicate that OTUB1 has dual functions that promote or suppress cancer. As expression of OTUB1 was dramatically enhanced by ^{211}At-MABG treatment (**Figure 6A**), OTUB1 is possibly a key enzyme in the tumor response to ^{211}At-MABG therapy in PCC.

Radiobiological insights and therapeutic mechanism of ^{211}At-MABG therapy

We should note that according to the half-life of 7.2 h, the cellular irradiation of α-particles lasted

longer than 12 minutes for ^{60}Co γ-ray irradiation (**Figure 7B**). The "low fluence rate" of α-particles in ^{211}At-MABG treatment was approximately "one α-particle emission in one hour on average" for the 10% iso-survival experiment (**Figure S2D; Supplementary result**). The low fluence rate may be linked to the avoidance of cell death because HR and non-homologous end-joining contributed to DSB repair in TAT [48]; our results also suggest the contribution of HR, *Fam175a* and *Rnf169* (**Table 1**). These findings raise the question regarding how anti-tumor therapeutic effects are induced at a low fluence rate, and the answer may be the p53 gene. Despite the low α-particle fluence rate, the p53 signaling pathway was overexpressed based on enrichment analysis (**Figure 4**), and p53 target genes related to cell cycle checkpoints and cell death—*Cdkn1a*, *Enc1*, *Tp53inp1*, *Ccng1*, *Plk2*, *Eda2r*, *Aen* and *Btg2*—were ranked among the representative DEGs (**Table 1-2**). In particular, gene expression for most of the p53-targeted genes—e.g., *Cdkn1a* in **Figure S7**—persisted and gradually increased over 3 time points. Possible causes may be due to p53-Mdm2 feedback [49] and OTUB1 [33, 47], both of which stabilize and sustain p53 signaling. Long-lasting p53-induced signaling may break the wall of the "low fluence rate" in PC12 tumor cell death to exert anti-tumor effects.

Study limitations

In this work, we have used PC12 as a representative cell-line for targeted radionuclide therapy, because PC12 is an important model cell-line for malignant pheochromocytoma study [15]. There is also a long history of nuclear medicine studies. In fact, the sufficient results of PC12 have contributed to the preclinical study of MIBG therapy, e.g. the report of Rutgers et al. [16]. On the other hand, human pheochromocytoma cell lines recently established such as KAT45 and hPhe01 may also be useful future target for this kind of study, as well as studies *in vivo* with Rat models to further validate the candidate response biomarkers.

Table 2. ^{211}At-MABG induced representative DEGs for decreased survival at all time points.

	All time points (5 genes)*1		
	Gene name	LogFC*2, *3	Function
Cell cycle	*Cdkn1a*	+1.680 (3)	G1/G2 checkpoint
Cell death	*Enc1*	+1.657 (4)	Negatively regulates autophagy, redox homeostasis
	Tp53inp1	+1.320 (5)	Apoptosis, Autophagy
Metastasis	*Gdf15*	+1.782 (1)	Epithelial mesenchymal transition
Others	*Fam212b*	+1.503 (2)	Unknown

*1 Number of DEGs. *2 The number in parentheses indicates the rank. *3 Value at 12 h post-treatment.

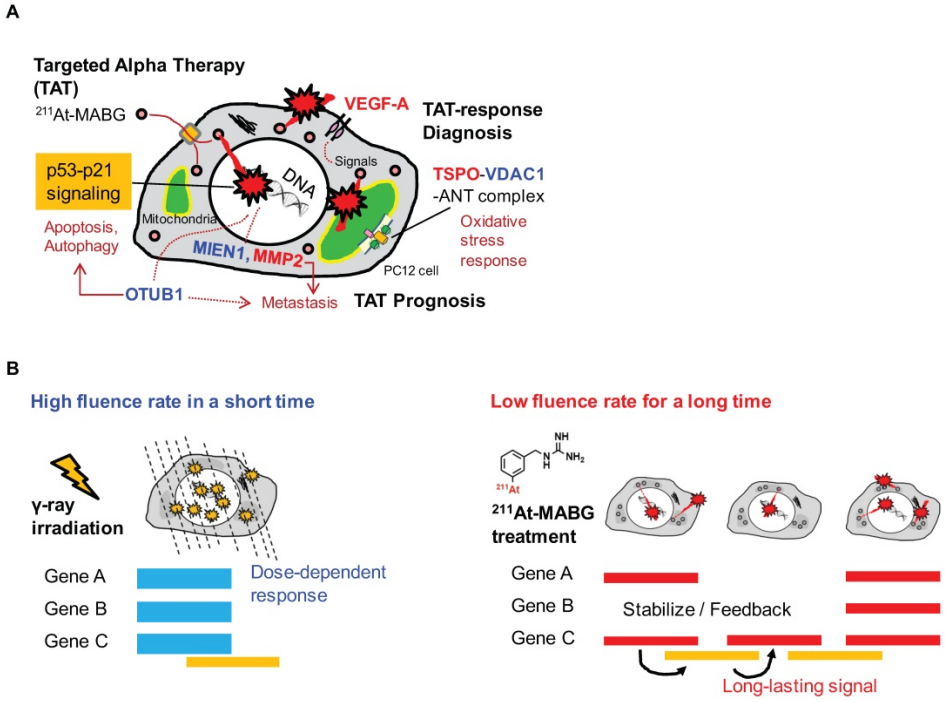

Figure 7. Potential biomarkers of ^{211}At-MABG-therapy and low fluence α-particle irradiation. (A) The present RNA-seq analysis suggests that ^{211}At-MABG therapeutic effects are associated with p53-p21 signaling and inhibition of ubiquitination by OTUB1. Furthermore, our analysis demonstrated novel targets for ^{211}At-MABG-therapy. OTUB1 and MIEN1 may be of importance for therapy and VDAC1 (TSPO) and VEGF-A for imaging. **(B)** Different irradiation modes of ^{60}Co γ-rays and α-particles emitted from ^{211}At-MABG. Photon radiation therapy uses high fluence-rate irradiation conducted in a short time and causes a biological response in a dose-dependent manner. In contrast, ^{211}At-MABG treatment is a mode of low fluence α-particle irradiation. The fluence rate was "one α-particle emission in one hour on average" for the 10% iso-survival experiment. Representative DEG analysis showed long-lasting p53-p21 signaling post-^{211}At-MABG treatment.

The present study was mainly based on RNA-seq analysis. Therefore, post-translational modifications (PTMs) such as glycosylation and phosphorylation were not examined. Further studies will be needed to address PTMs. In addition, we did not detect significant mutations in the *p53* gene in PC12 cells, though mutations in *p53* frequently occur in many cancers. The therapeutic molecular mechanism of *p53*-mutated tumor cells in TAT may be different from the present results, according to the type of mutation.

Conclusions

Our analysis demonstrated that ^{211}At-MABG therapeutic effects are associated with a molecular mechanism that occurs via the p53-p21 pathway, the *Otub1* gene related to ubiquitin-mediated proteolysis and other representative highly ranked DEGs. Additionally, we found 4 potential molecular biomarkers that can be used in molecular imaging and as therapeutic targets of ^{211}At-MABG-therapy.

Abbreviations

^{131}I-MIBG: *meta*-^{131}I-iodo-benzylguanidine; ^{211}At-MABG: *meta*-^{211}At-astato-benzylguanidine; DEGs: differentially expressed genes; FDR: false discovery rate; FPKM: fragments per kilobase of exon per million fragments mapped; IR: ionizing radiation; KEGG: Kyoto Encyclopedia of Genes and Genomes; NGS: next-generation sequencing; PCC: pheochromocytoma; RNA-seq: RNA-sequencing; *SF*: surviving fraction; TAT: targeted α therapy.

Supplementary Material

Supplementary figures and tables.
http://www.thno.org/v09p1538s1.pdf

Acknowledgements

This work was supported, in part, by research funds from the Yamagata Prefectural Government and Tsuruoka City, Japan. The authors thank Yuki Takai for technical assistance in sequencing, the staff of Takasaki ion accelerators for advanced radiation application and food irradiation facilities of QST for their operation.

Competing Interests

The authors have declared that no competing interest exists.

References

1. Lenders JW, Eisenhofer G, Mannelli M, Pacak K. Phaeochromocytoma. Lancet. 2005; 366(9486): 665-75.
2. Carrasquillo JA, Pandit-Taskar N, Chen CC. I-131 Metaiodobenzylguanidine Therapy of Pheochromocytoma and Paraganglioma. Semin Nucl Med. 2016; 46(3): 203-14.
3. Ohshima Y, Sudo H, Watanabe S, Nagatsu K, Tsuji AB, Sakashita T, et al. Antitumor effects of radionuclide treatment using α-emitting meta-^{211}At-astato-benzylguanidine in a PC12 pheochromocytoma model. Eur J Nucl Med Mol Imaging. 2018; 45(6): 999-1010.
4. Maier P, Hartmann L, Wenz F, Herskind C. Cellular Pathways in Response to Ionizing Radiation and Their Targetability for Tumor Radiosensitization. Int J Mol Sci. 2016; 17(1). pii: E102.
5. Pandya DN, Hantgan R, Budzevich MM, Kock ND, Morse DL, Batista I, et al. Preliminary Therapy Evaluation of ^{225}Ac-DOTA-c(RGDyK) Demonstrates that Cerenkov Radiation Derived from ^{225}Ac Daughter Decay Can Be Detected by Optical Imaging for *In Vivo* Tumor Visualization. Theranostics. 2016; 6(5): 698-709.
6. Nagao Y, Yamaguchi M, Watanabe S, Ishioka NS, Kawachi N, Watabe H. Astatine-211 imaging by a Compton camera for targeted radiotherapy. Appl Radiat Isot. 2018; 139: 238-243.
7. Paulmurugan R, Oronsky B, Brouse CF, Reid T, Knox S, Scicinski J. Real time dynamic imaging and current targeted therapies in the war on cancer: a new paradigm. Theranostics. 2013; 3(6): 437-47.
8. Wu C, Li F, Niu G, Chen X. PET imaging of inflammation biomarkers. Theranostics. 2013; 3(7): 448-66.
9. Koboldt DC, Steinberg KM, Larson DE, Wilson RK, Mardis ER. The next-generation sequencing revolution and its impact on genomics. Cell. 2013; 155(1): 27-38.
10. Wang Z, Gerstein M, Snyder M. RNA-Seq: a revolutionary tool for transcriptomics. Nat Rev Genet. 2009; 10(1): 57-63.
11. Seidl C, Port M, Apostolidis C, Bruchertseifer F, Schwaiger M, Senekowitsch-Schmidtke R, et al. Differential gene expression triggered by highly cytotoxic alpha-emitter-immunoconjugates in gastric cancer cells. Invest New Drugs. 2010; 28(1): 49-60.
12. Danielsson A, Claesson K, Parris TZ, Helou K, Nemes S, Elmroth K, et al. Differential gene expression in human fibroblasts after alpha-particle emitter ^{211}At compared with ^{60}Co irradiation. Int J Radiat Biol. 2013; 89(4): 250-8.
13. Yong KJ, Milenic DE, Baidoo KE, Brechbiel MW. Impact of α-targeted radiation therapy on gene expression in a pre-clinical model for disseminated peritoneal disease when combined with paclitaxel. PLoS One. 2014; 9(9): e108511.
14. Liu Y, Zhou J, White KP. RNA-seq differential expression studies: more sequence or more replication? Bioinformatics. 2014; 30(3): 301-4.
15. Eisenhofer G, Bornstein SR, Brouwers FM, Cheung NK, Dahia PL, et al. Malignant pheochromocytoma: current status and initiatives for future progress. Endocr Relat Cancer. 2004; 11(3): 423-36.
16. Rutgers M, Buitenhuis CK, van der Valk MA, Hoefnagel CA, Voûte PA, et al. [^{131}I] and [^{125}I] metaiodobenzylguanidine therapy in macroscopic and microscopic tumors: a comparative study in SK-N-SH human neuroblastoma and PC12 rat pheochromocytoma xenografts. Int J Cancer. 2000; 90(6): 312-25.
17. Shinohara A, Hanaoka H, Sakashita T, Sato T, Yamaguchi A, Ishioka NS, et al. Rational evaluation of the therapeutic effect and dosimetry of auger electrons for radionuclide therapy in a cell culture model. Ann Nucl Med. 2018; 32(2): 114-122.
18. Spetz J, Rudqvist N, Forssell-Aronsson E. Biodistribution and dosimetry of free ^{211}At, ^{125}I- and ^{131}I- in rats. Cancer Biother Radiopharm. 2013; 28(9): 657-64.
19. Herrera F, Lozano M, Verdegay JL. Tackling real-coded genetic algorithms: operators and tools for behavioural analysis. Artif Intell Rev. 1998; 12(4): 265–319.
20. Kim D, Pertea G, Trapnell C, Pimentel H, Kelley R, Salzberg SL. TopHat2: accurate alignment of transcriptomes in the presence of insertions, deletions and gene fusions. Genome Biol. 2013; 14(4): R36.
21. Trapnell C, Williams BA, Pertea G, Mortazavi A, Kwan G, van Baren MJ, et al. Transcript assembly and quantification by RNA-Seq reveals unannotated transcripts and isoform switching during cell differentiation. Nat Biotechnol. 2010; 28(5): 511-5.
22. Trapnell C, Hendrickson DG, Sauvageau M, Goff L, Rinn JL, Pachter L. Differential analysis of gene regulation at transcript resolution with RNA-seq. Nat Biotechnol 2013; 31: 46-53.
23. Moriya Y, Itoh M, Okuda S, Yoshizawa AC, Kanehisa M. KAAS: an automatic genome annotation and pathway reconstruction server. Nucleic Acids Res. 2007; 35(Web Server issue): W182-5.
24. Arakawa K, Mori K, Ikeda K, Matsuzaki T, Kobayashi Y, Tomita M. G-language Genome Analysis Environment: a workbench for nucleotide sequence data mining. Bioinformatics. 2003; 19(2): 305-6.
25. Buck JR, McKinley ET, Hight MR, Fu A, Tang D, Smith RA, et al. Quantitative, preclinical PET of translocator protein expression in glioma using ^{18}F-N-fluoroacetyl-N-(2,5-dimethoxybenzyl)-2-phenoxyaniline. J Nucl Med. 2011; 52(1): 107-14.
26. Abbas T, Dutta A. p21 in cancer: intricate networks and multiple activities. Nat Rev Cancer. 2009; 9(6): 400-14.
27. Sukhthankar M, Choi CK, English A, Kim JS, Baek SJ. A potential proliferative gene, NUDT6, is down-regulated by green tea catechins at the posttranscriptional level. J Nutr Biochem. 2010; 21(2): 98-106.
28. Tanikawa C, Furukawa Y, Yoshida N, Arakawa H, Nakamura Y, Matsuda K. XEDAR as a putative colorectal tumor suppressor that mediates p53-regulated anoikis pathway. Oncogene. 2009; 28(34): 3081-92.
29. Uyen B. Chu, Sevahn K. Vorperian, Kenneth Satyshur, Kelsey Eickstaedt, Nicholas V. Cozzi, Timur Mavlyutov, et al. Noncompetitive Inhibition of

Indolethylamine-*N*-methyltransferase by *N*,*N*-Dimethyltryptamine and *N*,*N*-Dimethylaminopropyltryptamine. Biochemistry. 2014; 53(18): 2956–2965.
30. Carbonaro TM, Gatch MB. Neuropharmacology of N,N-dimethyltryptamine. Brain Res Bull. 2016; 126(Pt 1): 74-88.
31. Fischer M. Census and evaluation of p53 target genes. Oncogene. 2017; 36(28): 3943-3956.
32. Kpetemey M, Chaudhary P, Van Treuren T, Vishwanatha JK. MIEN1 drives breast tumor cell migration by regulating cytoskeletal-focal adhesion dynamics. Oncotarget. 2016; 7(34): 54913-54924.
33. Sun XX, Dai MS. Deubiquitinating enzyme regulation of the p53 pathway: A lesson from Otub1. World J Biol Chem. 2014; 5(2): 75-84.
34. Baietti MF, Simicek M, Abbasi Asbagh L, Radaelli E, Lievens S, Crowther J, et al. OTUB1 triggers lung cancer development by inhibiting RAS monoubiquitination. EMBO Mol Med. 2016; 8(3): 288-303.
35. Gatliff J, Campanella M. TSPO is a REDOX regulator of cell mitophagy. Biochem Soc Trans. 2015; 43(4): 543-52.
36. Gaykema SB, Brouwers AH, Lub-de Hooge MN, Pleijhuis RG, Timmer-Bosscha H, Pot L, et al. ^{89}Zr-bevacizumab PET imaging in primary breast cancer. J Nucl Med. 2013; 54(7): 1014-8.
37. Backer MV, Backer JM. Imaging key biomarkers of tumor angiogenesis. Theranostics. 2012; 2(5): 502-15.
38. Forsythe JA, Jiang BH, Iyer NV, Agani F, Leung SW, Koos RD, et al. Activation of vascular endothelial growth factor gene transcription by hypoxia-inducible factor 1. Mol Cell Biol. 1996; 16(9): 4604-13.
39. Mezquita P, Parghi SS, Brandvold KA, Ruddell A. Myc regulates VEGF production in B cells by stimulating initiation of VEGF mRNA translation. Oncogene. 2005; 24(5): 889-901.
40. Ren F, Tang R, Zhang X, Madushi WM, Luo D, Dang Y, et al. Overexpression of MMP Family Members Functions as Prognostic Biomarker for Breast Cancer Patients: A Systematic Review and Meta-Analysis. PLoS One. 2015; 10(8): e0135544.
41. Valkovskaya N, Kayed H, Felix K, Hartmann D, Giese NA, Osinsky SP, et al. ADAM8 expression is associated with increased invasiveness and reduced patient survival in pancreatic cancer. J Cell Mol Med. 2007; 11(5): 1162-74.
42. Chen J, Deng L, Dreymüller D, Jiang X, Long J, Duan Y, et al. A novel peptide ADAM8 inhibitor attenuates bronchial hyperresponsiveness and Th2 cytokine mediated inflammation of murine asthmatic models. Sci Rep. 2016; 6: 30451.
43. Ende C, Gebhardt R. Inhibition of matrix metalloproteinase-2 and -9 activities by selected flavonoids. Planta Med. 2004; 70(10): 1006-8.
44. Xu Q, Xu HX, Li JP, Wang S, Fu Z, Jia J, et al. Growth differentiation factor 15 induces growth and metastasis of human liver cancer stem-like cells via AKT/GSK-3β/β-catenin signaling. Oncotarget. 2017; 8(10): 16972-16987.
45. Haipeng Ren, Yuanling Qi, Xiaoyan Yin, Jianfeng Gao. miR-136 targets MIEN1 and involves the metastasis of colon cancer by suppressing epithelial-to-mesenchymal transition. Onco Targets Ther. 2018; 11: 67–74.
46. Chen Y, Wang YG, Li Y, Sun XX, Dai MS. Otub1 stabilizes MDMX and promotes its proapoptotic function at the mitochondria. Oncotarget. 2017; 8(7): 11053-11062.
47. Wang Y, Zhou X, Xu M, Weng W, Zhang Q, Yang Y, et al. OTUB1-catalyzed deubiquitination of FOXM1 facilitates tumor progression and predicts a poor prognosis in ovarian cancer. Oncotarget. 2016; 7(24): 36681-36697.
48. Song H, Hedayati M, Hobbs RF, Shao C, Bruchertseifer F, Morgenstern A, et al. Targeting aberrant DNA double-strand break repair in triple-negative breast cancer with alpha-particle emitter radiolabeled anti-EGFR antibody. Mol Cancer Ther. 2013; 12(10): 2043-54.
49. Moll UM, Petrenko O. The MDM2-p53 interaction. Mol Cancer Res. 2003; 1(14): 1001-8.